

# Superfluidity and pairing phenomena in ultracold atomic Fermi gases in one-dimensional optical lattices. I. Balanced case

Jibiao Wang,<sup>1,2</sup> Leifeng Zhang,<sup>2</sup> Yi Yu,<sup>3</sup> Chaohong Lee ,<sup>1,4</sup> and Qijin Chen <sup>5,2,6,\*</sup>

<sup>1</sup>Guangdong Provincial Key Laboratory of Quantum Metrology and Sensing & School of Physics and Astronomy, Sun Yat-Sen University (Zhuhai Campus), Zhuhai, Guangdong 519082, China

<sup>2</sup>Department of Physics and Zhejiang Institute of Modern Physics, Zhejiang University, Hangzhou, Zhejiang 310027, China

<sup>3</sup>College of Chemical Engineering, Zhejiang University of Technology, Hangzhou, Zhejiang 310014, China

<sup>4</sup>State Key Laboratory of Optoelectronic Materials and Technologies, Sun Yat-Sen University (Guangzhou Campus), Guangzhou, Guangdong 510275, China

<sup>5</sup>Shanghai Branch, National Laboratory for Physical Sciences at Microscale and Department of Modern Physics, University of Science and Technology of China, Shanghai 201315, China

<sup>6</sup>Synergetic Innovation Center of Quantum Information and Quantum Physics, Hefei, Anhui 230026, China



(Received 15 January 2020; accepted 7 April 2020; published 11 May 2020)

The superfluidity and pairing phenomena in ultracold atomic Fermi gases have been of great interest in recent years, with multiple tunable parameters. Here we study the BCS-BEC crossover behavior of balanced two-component Fermi gases in a one-dimensional optical lattice, which is distinct from the simple three-dimensional (3D) continuum and a fully 3D lattice often found in a condensed matter system. We use a pairing fluctuation theory which includes self-consistent feedback effects at finite temperatures and find widespread pseudogap phenomena beyond the BCS regime. As a consequence of the lattice periodicity, the superfluid transition temperature  $T_c$  decreases with pairing strength in the BEC regime, where it approaches asymptotically  $T_c = \pi a n / 2m$ , with  $a$  being the  $s$ -wave scattering length, and  $n$  ( $m$ ) the fermion density (mass). In addition, the quasi-two dimensionality leads to fast-growing (absolute value of the) fermionic chemical potential  $\mu$  and pairing gap  $\Delta$ , which depends exponentially on the ratio  $d/a$ . Importantly,  $T_c$  at unitarity increases with the lattice constant  $d$  and hopping integral  $t$ . The effect of the van Hove singularity on  $T_c$  is identified. The superfluid density exhibits  $T^{3/2}$  power laws at low  $T$ , away from the extreme BCS limit. These predictions can be tested in future experiments.

DOI: [10.1103/PhysRevA.101.053617](https://doi.org/10.1103/PhysRevA.101.053617)

## I. INTRODUCTION

Ultracold atomic Fermi gases loaded in optical lattices have attracted enormous attention in condensed matter and atomic, molecular, and optical (AMO) physics [1–3]. With multiple easily tunable parameters, they become more and more important as a quantum simulator nowadays [4–6]. Fermions in *pure* optical lattices are often described by a Hubbard model [5–7]. Among them, the one-dimensional (1D) case can be solved exactly via the Bethe ansatz [8]. However, while for a 1D Hubbard model each site has at most two fermions, the 1D optical lattice is actually rather different; each site in the lattice direction corresponds to a 2D plane in the transverse dimensions and thus can accommodate many fermions. Therefore, a 1D optical lattice is a quasi-2D or 3D system [9,10], depending on the lattice parameters. Moreover, the genuine 1D Hubbard model does not possess a long-range order; hence, it cannot support a superfluid phase. In contrast, fermions trapped in 1D optical lattices can not only form a superfluid [11,12], but also exhibit interesting pseudogap phenomena in the normal state [13]. A condensed matter analog

of the 1D optical lattice is the superlattice of semiconductor heterostructures such as the AlGaAs/GaAs/InGaAs structure, except now we are considering pairing phenomena under a tunable attractive interaction.

Including the Hubbard model, there has been extensive literature on 3D (and 2D or 1D) lattices in the field of condensed matter [14,15]. Most of these existing Hubbard-model-based works address pure lattice cases, since the kinetic energy term often contains only the lattice site hopping [7,16–20]. The “1D optical lattice” in many theoretical works in the literature refers to a genuine 1D lattice in the traditional sense [21]. While both types of lattices can now be realized experimentally, to avoid possible confusions, *we emphasize that, by 1D optical lattice, here we mean a periodic stack of 2D planes*, and therefore it is a mix of continuum in the transverse 2D  $xy$  planes and lattice discreteness in the longitudinal  $z$  direction.

Such 1D optical lattices can be readily realized experimentally. However, theoretical studies on these systems have been scarce. Devreese *et al.* studied possible Fulde-Ferrell-Larkin-Ovchinnikov (FFLO) states [22,23] in such a 1D optical lattice [24]. Like many others in the literature [7], when studying population imbalance effects, they use the fermion chemical potential  $\mu$  and the chemical potential difference  $h$  as control

\*qchen@zju.edu.cn

variables. While this choice makes numerical calculations simpler, it often restricts the study to the (weak coupling) BCS and (intermediate coupling) crossover regimes. Indeed, the superfluid and pairing physics in a 1D optical lattice has not been adequately studied thus far. Given the various available tuning parameters, including the pairing interaction strength, lattice constant and depth, fermion density, population imbalance, as well as mass imbalance in the case of a Fermi-Fermi mixture, there are certainly many facets of the phase diagram and associated very rich physics. In particular, one would like to know if there are exotic new phases emerging, and how to properly characterize such a 1D optical lattice.

In this paper, we study two-component fermions loaded in 1D optical lattices using a pairing fluctuation theory, which has been applied successfully to various BCS–Bose-Einstein condensation (BEC) crossover phenomena [4,25–27], including in quasi-two-dimensional (quasi-2D) and 3D optical lattices [15,17,28]. These systems can be quasi-2D or 3D, depending on the lattice constant  $d$  and hopping integral  $t$  [29], as well as the pairing strength. Due to the complexity induced by multiple tunable parameters, in this paper (Part I), we restrict ourselves to population (and mass) balanced cases only. Here we consider the combined effects of lattice constant, hopping integral, and interaction strength. We find that the mixing between continuum and discrete lattice dimensions leads to exponential behavior of the fermionic chemical potential  $\mu$  and the pairing gap  $\Delta$  as a function of  $d/a$  in the BEC regime ( $1/k_F a \gg 1$ ), where  $k_F$  is the Fermi momentum and  $a$  is the two-body  $s$ -wave scattering length, in contrast to the power laws in the pure 3D continuum or 3D lattice cases. We shall present detailed phase diagrams as the system undergoes the BCS-BEC crossover with different lattice constants and hopping integrals, and mainly focus on the finite temperature effects, especially the pseudogap phenomena [30,31]. These phase diagrams reveal the following: (i) The pseudogap phenomena widely exist; (ii) at unitarity,  $T_c$  increases with the increase of lattice constant or hopping integral; (iii) as a consequence of the lattice periodicity,  $T_c$  decreases with pairing strength in the BEC regime and approaches asymptotically  $T_c = \pi a n / 2m$ , where  $n$  is the atom number density and  $m$  is the atomic mass; (iv) in addition, the quasi-two dimensionality leads to fast-growing (absolute value of the) fermionic chemical potential  $\mu$  and pairing gap  $\Delta$ , which depends exponentially on the ratio  $d/a$ ; (v) due to the contribution of finite momentum pairs, the temperature dependence of the superfluid density  $n_s/m$  at low  $T$  evolves from exponential in the extreme BCS limit ( $1/k_F a \ll -1$ ) to a simple  $T^{3/2}$  power law in the BEC regime ( $\mu < 0$ ), for both the in-plane and the out-of-plane (lattice) components.

## II. THEORETICAL FORMALISM

### A. General theory

While the in-plane ( $xy$  directions) motion of the fermions has a free parabolic dispersion, we use a one-band nearest-neighbor tight-binding model for the out-of-plane lattice dimension ( $z$  direction), with the single-particle dispersion given by  $\xi_{k\sigma} = \mathbf{k}_{\parallel}^2 / 2m + 2t[1 - \cos(k_z d)] - \mu_{\sigma} \equiv \epsilon_{\mathbf{k}} - \mu_{\sigma}$ . Here  $\mathbf{k}_{\parallel} \equiv (k_x, k_y)$  and  $t$  is the hopping integral between

neighboring lattice sites,  $d$  the optical lattice constant, and  $\mu_{\sigma}$  the fermionic chemical potentials for two (pseudo)spins  $\sigma = \uparrow, \downarrow$ . In the absence of imbalance, we have  $\mu_{\sigma} = \mu$  and  $\xi_{k\sigma} = \xi_{\mathbf{k}}$ , and we shall drop the spin indices. We restrict  $k_z$  to the first Brillouin zone (BZ)  $[-\pi/d, \pi/d]$  due to the lattice periodicity and set the volume  $V = 1$ ,  $\hbar = k_B = 1$ . The one-band approximation is justified when the band gap is tuned large. The fundamental formalism of the pairing fluctuation theory for the present work is the same as that given in Refs. [4,25], except that we need to rederive the equations with the continuum-lattice mixed dispersion. To keep this paper self-contained, here we recapitulate the derivation and main equations.

The (inverse) bare Green's function is given by  $G_0^{-1}(K) = i\omega_n - \xi_{\mathbf{k}}$ , with the self-energy  $\Sigma(K) = \sum_Q t(Q)G_0(Q - K)$ . Following Ref. [25], we use a four-vector notation,  $\sum_K \equiv T \sum_n \sum_{\mathbf{k}}$ ,  $\sum_Q \equiv T \sum_l \sum_{\mathbf{q}}$ , and  $K \equiv (i\omega_n, \mathbf{k})$ ,  $Q \equiv (i\Omega_l, \mathbf{q})$ , where  $\omega_n = (2n + 1)\pi T$ ,  $\Omega_l = 2l\pi T$  are odd and even Matsubara frequencies, respectively [32]. At finite  $T$ , the  $T$ -matrix  $t(Q)$  contains a contribution from condensed pairs  $t_{sc}(Q)$  and noncondensed pairs  $t_{pg}(Q)$ , with  $t(Q) = t_{sc}(Q) + t_{pg}(Q)$ , where  $t_{sc}(Q) = -(\Delta_{sc}^2/T)\delta(Q)$  vanishes for  $T > T_c$ , and  $t_{pg}(Q) = U/[1 + U\chi(Q)]$ , with the short range  $s$ -wave pairing interaction pairing strength  $U < 0$  and the pair susceptibility  $\chi(Q) = \sum_K G_0(Q - K)G(K)$ . Here  $G(K)$  is the full Green's function, with the self-energy given by  $\Sigma(K) = \Sigma_{sc}(K) + \Sigma_{pg}(K)$ , where  $\Sigma_{sc}(K) = \sum_Q t_{sc}(Q)G_0(Q - K) = -\Delta_{sc}^2 G_0(-K)$ , and  $\Sigma_{pg}(K) = \sum_Q t_{pg}(Q)G_0(Q - K)$ . At  $T \leq T_c$ , the generalized Thouless criterion [33], or equivalently BEC condition for pairs, requires  $t_{pg}^{-1}(Q=0) = U^{-1} + \chi(0) = 0$ . This implies that  $t_{pg}(Q)$  is dominated by the vicinity of  $Q=0$ , so that  $\Sigma_{pg}(K)$  may be approximated by  $\Sigma_{pg}(K) \approx \sum_Q t_{pg}(Q)G_0(-K) \equiv -\Delta_{pg}^2 G_0(-K)$ , where  $\Delta_{pg}^2 \equiv -\sum_Q t_{pg}(Q)$  and we have discarded the incoherent background part of the self energy. (The parameter  $\Delta_{pg}$  is referred to as pseudogap, as is widely found in cuprate superconductors [34].) Then the total self-energy  $\Sigma(K)$  takes the simple BCS-like form,  $\Sigma(K) = -\Delta^2 G_0(-K)$ , where  $\Delta^2 = \Delta_{sc}^2 + \Delta_{pg}^2$ . Finally, the Dyson's equation  $G^{-1}(K) = G_0^{-1}(K) - \Sigma(K)$  leads immediately to the full Green's function

$$G(K) = \frac{u_{\mathbf{k}}^2}{i\omega_n - E_{\mathbf{k}}} + \frac{v_{\mathbf{k}}^2}{i\omega_n + E_{\mathbf{k}}}, \quad (1)$$

where  $u_{\mathbf{k}}^2 = (1 + \xi_{\mathbf{k}}/E_{\mathbf{k}})/2$ ,  $v_{\mathbf{k}}^2 = (1 - \xi_{\mathbf{k}}/E_{\mathbf{k}})/2$ , and  $E_{\mathbf{k}} = \sqrt{\xi_{\mathbf{k}}^2 + \Delta^2}$ . From the number constraint  $n = 2 \sum_K G(K)$ , we can get the fermion number density

$$n = 2 \sum_{\mathbf{k}} \left[ v_{\mathbf{k}}^2 + f(E_{\mathbf{k}}) \frac{\xi_{\mathbf{k}}}{E_{\mathbf{k}}} \right], \quad (2)$$

where  $f(x) = 1/(e^{x/T} + 1)$  is the Fermi distribution function.

Above  $T_c$ , the Thouless criterion should be modified by  $U^{-1} + \chi(0) = a_0 \mu_p$ , where  $\mu_p$  is the effective pair chemical potential and  $a_0$  is the coefficient of the linear  $\Omega$  term in the Taylor expansion of the inverse  $T$ -matrix (see below) [4]. This

leads to the extended gap equation

$$\frac{m}{4\pi a} = \sum_{\mathbf{k}} \left[ \frac{1}{2\epsilon_{\mathbf{k}}} - \frac{1 - 2f(E_{\mathbf{k}})}{2E_{\mathbf{k}}} \right] + a_0\mu_p, \quad (3)$$

with  $\mu_p = 0$  at  $T \leq T_c$ . Here, the coupling strength  $U$  has been replaced by the  $s$ -wave scattering length  $a$  via  $U^{-1} = m/4\pi a - \sum_{\mathbf{k}} 1/2\epsilon_{\mathbf{k}}$ . Note that this scattering length is different from that defined in simple 3D free space, since  $k_z$  is now restricted to within the first BZ. We caution that it does *not* necessarily yield the experimentally measured scattering length. One can define an effective scattering length via  $a_{\text{eff}} = a/\sqrt{2mt_d}$ , which is more comparable to the physical scattering length. For details, see Appendices A and B. It should also be noted that we have implicitly assumed a negative  $U$  model for the lattice direction and the on-site  $U$  is same as the in-plane pairing strength  $U$ . In real space, the pairing interaction is given by  $U(\mathbf{r}, \mathbf{r}') = U\delta(x-x')\delta(y-y')\delta_{ij}$ , where  $i, j$  is the lattice site index in the  $\hat{z}$  direction.

The inverse  $T$ -matrix expansion [4], after analytic continuation ( $i\Omega_l \rightarrow \Omega + i0^+$ ), is given by

$$t_{\text{pg}}^{-1}(\Omega, \mathbf{q}) \approx a_1\Omega^2 + a_0(\Omega - \Omega_{\mathbf{q}} + \mu_p), \quad (4)$$

with  $\Omega_{\mathbf{q}} = B_{\parallel}\mathbf{q}_{\parallel}^2 + 2t_B[1 - \cos(q_z d)]$ . Here  $B_{\parallel} = 1/2M_{\parallel}$ , with  $M_{\parallel}$  being the effective pair mass in the  $xy$  plane, and  $t_B$  is the effective hopping integral for noncondensed pairs. The  $a_1$  term serves as a small quantitative correction; except in the weak coupling BCS regime, we have  $a_1 T_c \ll a_0$ . The coefficients  $a_1, a_0, B_{\parallel}$  and  $t_B$  can be derived from the pair susceptibility via straightforward Taylor expansion, as given in Appendix C. Consequently, we have the pseudogap equation

$$a_0\Delta_{\text{pg}}^2 = \sum_{\mathbf{q}} \frac{b(\tilde{\Omega}_{\mathbf{q}})}{\sqrt{1 + 4\frac{a_1}{a_0}(\Omega_{\mathbf{q}} - \mu_p)}}, \quad (5)$$

where  $b(x)$  is the Bose distribution function and  $\tilde{\Omega}_{\mathbf{q}} = \sqrt{a_0^2[1 + 4a_1(\Omega_{\mathbf{q}} - \mu_p)/a_0] - a_0}/2a_1$  is the pair dispersion. When  $a_1/a_0$  is small, we have  $\tilde{\Omega}_{\mathbf{q}} = \Omega_{\mathbf{q}} - \mu_p$ . Then  $a_0\Delta_{\text{pg}}^2$  yields the density of finite momentum pairs. Including the condensate, the total pair density is given by  $n_p = a_0\Delta^2$ .

Equations (2)–(5) form a closed set of self-consistent equations, which can be used to solve for  $(\mu, T^*)$  with  $\Delta = 0$ , for  $(\mu, \Delta_{\text{pg}}, T_c)$  with  $\Delta_{\text{sc}} = 0$ , and for  $(\mu, \Delta, \Delta_{\text{pg}})$  at  $T < T_c$ . Here the pair formation temperature  $T^*$  is approximated by the mean-field  $T_c$ , and the order parameter  $\Delta_{\text{sc}}$  can be derived from  $\Delta_{\text{sc}}^2 = \Delta^2 - \Delta_{\text{pg}}^2$  below  $T_c$ .

### B. Asymptotic behavior in the deep BEC regime

In the deep BEC regime,  $\mu \rightarrow -\infty$ . The integrals in the equations can be performed analytically using Taylor expansions. The fermion number equations reduce to

$$n = -\frac{m\Delta^2}{4\pi\mu d} \quad \text{or} \quad \Delta = \sqrt{\frac{4\pi|\mu|dn}{m}}. \quad (6)$$

With the help of Eq. (6), the chemical potential  $\mu$  can be uniquely determined by the gap equations. Then  $\mu$  and the gap  $\Delta$  are given by

$$\mu = -te^{d/a} + 2t + \frac{2\pi dn}{m}, \quad (7)$$

$$\Delta = 2\sqrt{\frac{\pi t dn}{m}} e^{d/2a} \left( 1 - \frac{\pi dn}{mt} e^{-d/a} \right). \quad (8)$$

Note that the exponential behavior of  $\mu$  and  $\Delta$  as a function of  $1/k_F a$  is an important feature of the quasi-two dimensionality of the continuum-lattice mixed system. This should be contrasted with the corresponding behaviors in the 3D continuum and 3D lattices, where power law dependencies are found. In particular, a 3D continuum has the scaling relation  $\Delta \sim |\mu|^{1/4}$  in the BEC regime and thus  $\Delta^2/\mu$  decreases with  $1/k_F a$ . On the other hand for a 3D lattice, due to the finite volume of the unit cell, both  $|\mu|$  and  $\Delta$  grow linearly with  $|U|$ , with a ratio of  $\Delta/|\mu| = \sqrt{2n - n^2}/(1 - n)$  for  $n < 1$  per unit cell. In contrast, for the present continuum-lattice mixed system, the ratio  $\Delta^2/\mu$  approaches a constant, independent of pairing strength. For this reason, the (2nd and 3rd) correction terms in Eq. (7) are also constants, independent of the interaction strength. The correction term in Eq. (8) quickly drops as  $|U|$  increases.

To solve for  $T_c$ , we first derive the pair dispersion, and find

$$B_{\parallel} = \frac{1}{4m}, \quad (9)$$

$$t_B = \frac{t^2}{2|\mu|} \approx \frac{t}{2} e^{-d/a}. \quad (10)$$

While the in-plane pair mass in the BEC regime is given by  $2m$ , as expected, the out-of-plane pair mass becomes exponentially heavy, as a function of increasing  $d/a$ . This can be easily understood since on a lattice pairs hop mainly via “virtual ionization” [35] (i.e., virtual pair unbinding) and thus its mobility is inversely proportional to the pair binding energy  $2|\mu|$ . The pseudogap equation now becomes the equation for pair density  $n_p$ ,

$$a_0\Delta^2 \equiv n_p = \frac{n}{2}, \quad (11)$$

and the coefficient  $a_1$  is given by

$$a_1\Delta^2 = -\frac{n}{8\mu}, \quad (12)$$

which becomes exponentially small in the BEC limit. Now one readily derive the solution for  $T_c$ ,

$$T_c = \frac{2\pi B_{\parallel} dn}{d/a - \ln(t/T_c)} \approx \frac{\pi an}{2m} = \frac{k_F a}{3\pi} T_F, \quad (13)$$

where use has been made of the definition of  $k_F = (3\pi^2 n)^{1/3}$  and  $E_F = T_F = k_F^2/2m$  (as in 3D continuum) in the last step, and we have dropped the small logarithmic correction  $\ln(t/T_c)$  in the denominator. An important and interesting aspect of this result is that *the BEC asymptote is essentially independent of  $d$* , and the effect of  $t$  only enters through a logarithmic correction, which can be safely neglected in the asymptote as well.

Equation (10) manifests a 3D to 2D crossover; as  $t$  decreases or  $d$  increases, the out-of-plane pair hopping integral  $t_B$  decreases rapidly while the in-plane effective pair mass remains unaffected. At the same time, the underlying fermions also experience a 3D to 2D crossover as  $t$  decreases [29]. In the quasi-2D regime, the kinetic energy of both fermions and pairs come mainly from in-plane motion. In the extreme quasi-2D limit, where  $t$  is tiny, the logarithmic correction  $\ln(t/T_c)$  in Eq. (13) will no longer be small. As a result,  $T_c$  vanishes logarithmically as a function of  $t$ . Indeed, the 2D limit is realized when the connections between different 2D layers become negligible, and this makes the lattice equivalent to a single tightly confined 2D plane, which has been actively studied both experimentally [13,36] and theoretically [37]. In this case, the Berezinskii-Kosterlitz-Thouless (BKT) transition [38] may come into play [39]. Note, however, that the logarithmic dependence of  $T_c$  on  $t$  requires an exponentially small  $t$  to access the exact 2D limit.

In the extreme quasi-2D cases, one may define a 2D scattering length  $a_{2D}$  via the two-body binding energy  $\epsilon_B$  as in exact 2D. To keep Eq. (7) valid, for given  $a_{2D}$ ,  $1/k_F a$  has to diverge logarithmically as a function of  $t$ , following Eq. (A4). See Appendix A for more details.

### C. Superfluid density

Given the solution of the self-consistent equations, one can easily investigate the transport behavior of the system. As an example, in this subsection, we shall present calculations for superfluid “density”  $n_s/m$ , which is important quantity in the superfluid phase. In superconductors, it is often measured via the London penetration depth  $\lambda_L$ , especially at low  $T$ , with the relation  $n_s/m \propto \lambda_L^{-2}$ . The temperature dependence at low  $T$  often serves as a strong indicator for the pairing symmetry of a superconductor, as it depends strongly on the pairing symmetry. BCS mean-field calculations show that it exhibits exponential  $T$  dependence for an  $s$ -wave superconductor, and linear  $T$  dependence for a nodal  $d$ -wave superconductor [25,34,40–42].

The expression for superfluid density can be derived following Refs. [25,43], using the linear response theory. More technical details can be found in Ref. [44]. For the present charge-neutral atomic gases, we only need to assume a fictitious vector potential, which can actually be realized experimentally via synthetic gauge fields.

Without imbalance, the superfluid density is given by

$$\left(\frac{n_s}{m}\right)_i = 2 \sum_{\mathbf{k}} \frac{\Delta_{sc}^2}{E_{\mathbf{k}}^2} \left[ \frac{1 - 2f(E_{\mathbf{k}})}{2E_{\mathbf{k}}} + f'(E_{\mathbf{k}}) \right] \left( \frac{\partial \xi_{\mathbf{k}}}{\partial k_i} \right)^2, \quad (14)$$

where  $i = x, y, z$  and  $f'(x) = -f(x)f(-x)/T$  is the directive of the Fermi distribution function.

Following Ref. [44], it can be shown that for the in-plane motion,  $(n_s/m)_{\parallel} = (n_s/m)_x = (n_s/m)_y = n/m$  at  $T = 0$ , since  $\partial^2 \xi_{\mathbf{k}} / \partial k_i^2 = 1/m = \text{const}$  for  $i = x, y$ . In contrast, in the lattice direction, the inverse band mass  $(1/m)_z = \partial^2 \xi_{\mathbf{k}} / \partial k_z^2 = 2td^2 \cos(k_z d)$  is  $k_z$  dependent and scaled by the factor  $td^2$ . As a consequence, we expect  $(n_s/m)_z \propto t^2 d^2$  and becomes small for realistic lattices, based on Eq. (14).

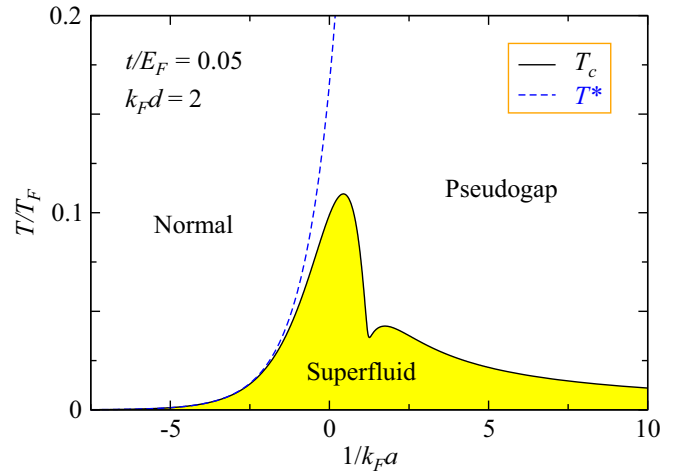


FIG. 1. Typical phase diagram in the  $T - 1/k_F a$  plane, calculated for  $t/E_F = 0.05$  and  $k_F d = 2$ .

## III. NUMERICAL RESULTS AND DISCUSSIONS

### A. Effect of lattice-continuum mixing on BCS–BEC crossover

In this subsection, we first investigate the effect of lattice-continuum mixing on the behavior of  $T_c$  and phase diagram throughout the BCS–BEC crossover regimes.

Shown in Fig. 1 is a typical phase diagram of a two-component balanced Fermi gas in a 1D optical lattice. Here we take realistic values for  $t$  and  $d$ , with  $t/E_F = 0.05$  and  $k_F d = 2$ . Note that in the zero lattice depth limit, the fermion energy in the lattice dimension should reduce to the simple parabolic dispersion, with mass  $m$ . Therefore, we set  $td^2 < 1/2m$  as a constraint on the choice of the values of  $t$  and  $d$ . Here we have  $2mtd^2 = 0.2$ . The (yellow) shaded area is the superfluid phase, whereas the (blue) dashed curve is the mean-field solution of  $T_c$ . We take this as an estimate of the pair formation temperature,  $T^*$ . Between the  $T^*$  and  $T_c$  curves, there exists the pseudogap phase, where incoherent pairs exist but without phase coherence or Bose condensation. The  $T_c$  curve reaches a maximum in the vicinity of unitarity, where  $1/k_F a = 0$ . In the BEC regime,  $T_c$  decreases with increasing pairing strength. Note that the existence of the pseudogap phase is an inevitable feature of the BCS–BEC crossover.

This phase diagram looks qualitatively similar to that in a 3D or quasi-2D pure lattice [15,28]. However, we note that it in fact exhibits features of both pure 3D continuum and pure lattice cases. On the one hand, there is a minimum in  $T_c$  around where the fermionic chemical potential  $\mu$  changes sign, a feature of 3D continuum [15,45]. On the other hand, the decrease of  $T_c$  with increasing  $1/k_F a$  in the BEC regime is a feature of pair hopping via virtual pair unbinding-rebinding processes [15,35] in a lattice. The BEC regime is not accessible at high densities in a 3D or quasi-2D pure lattice. In a typical 3D lattice, the minimum disappears, leaving only a kink as a residue of the minimum [28]. In a quasi-2D lattice, such a minimum may exist only in the low density regime, where the inter-particle distance becomes much larger than the lattice constant. Indeed, the present system with an in-plane continuum space should be comparable to the low density limit when compared to the quasi-2D lattice case.

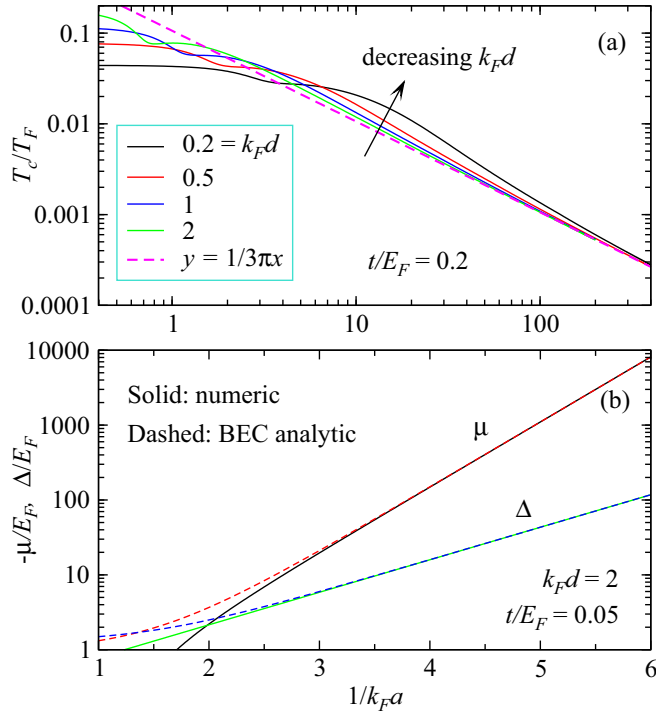


FIG. 2. Comparison between fully numerical and analytical solutions in the BEC regime for (a)  $T_c$  and (b) corresponding  $\mu$  and  $\Delta$  at  $T_c$ , as a function of  $1/k_F a$ . Shown in (a) are log-log plots of  $T_c$  (solid lines) for  $t/E_F = 0.2$  and varying  $k_F d$  from 0.2 to 2, while the dashed line represents the analytical solution, Eq. (13). Plotted in (b) are  $-\mu$  and  $\Delta$  in a semilog scale for  $t/E_F = 0.05$  and  $k_F d = 2$ , where the analytical solutions (dashed lines) are given by Eqs. (7) and (8).

There are further distinctions between the present lattice-continuum mix and the pure systems. In Fig. 2, we show the comparison between the fully numerical and analytical solutions of (a)  $T_c$  and (b)  $\mu$  as a function of  $1/k_F a$  in the BEC regime. Shown in Fig. 2(a) are the  $T_c$  curves in log-log scales for different values of  $d$ , while keeping  $t$  fixed at  $t = 0.2E_F$ . Also shown is the analytical solution, Eq. (13), in the BEC regime (magenta dashed line). As is evident, all  $T_c$  curves approach this  $(t, d)$ -independent analytical solution in the deep BEC regime. The larger  $d$  case converges faster.

In Fig. 2(b), we present a semilog plot of  $-\mu$  and  $\Delta$  as a function of  $1/k_F a$  for  $t = 0.05E_F$  and  $k_F d = 2$ , and compare the fully numerical solutions (solid lines) with the analytic expressions (dashed lines) given by Eqs. (7) and (8). As can be readily seen for the present case, the analytical expressions become a very good approximation for the fully numerical solutions for  $1/k_F a > 3$ .

From Fig. 2, we demonstrate that  $T_c$  scales proportionally with  $k_F a = (1/k_F a)^{-1}$  in the BEC regime, following Eq. (13). This is different from its counterpart relation,  $T_c \sim 1/U$ , in a pure 3D lattice [15,35]. While the general trend is the same, however, one does not have  $1/k_F a \propto U$  in the strong coupling limit.

The parameters  $t$  and  $d$  are the decisive factors for the shape of the Fermi surface. This can be seen from that of the lattice component in Fig. 1 of Ref. [29]. When  $t$  is small, the first BZ of the lattice dimension will be fully occupied.

In this case, a small  $d$  means a large phase space  $\pm\pi/d$  in the lattice direction, and therefore, will bring down the Fermi level as more particles now occupy the small  $k_{\parallel}$  but large  $|k_z|$  states. On the contrary, a large  $d$  will compress the phase space region between  $\pm\pi/d$ , and thus will push up the (in-plane) Fermi level. This can be understood from the real space perspective as well. As  $d$  increases, the spacing between neighboring planes increases. Therefore, the area density within each plane has to increase accordingly to keep the overall average 3D density fixed. In this way, the Fermi level will be pushed up to  $\mu_0 = \sqrt{2\pi n_{2D}}$ , where  $n_{2D}$  is the 2D fermion number density per plane. However, for a larger  $t$ , it may be possible that the first BZ in the  $z$  direction is not fully occupied. The Fermi surface in the  $z$  direction will allow a larger dispersion when  $t$  increases. Depending on the size of  $(t, d)$ , the Fermi surface may possess a shape of an ellipsoid, a disk, a cylinder, or something in between. Except for the ellipsoid, all other types of Fermi surfaces are open. A van Hove singularity will appear at the Fermi level at the topological transition point between open and closed Fermi surfaces.

Now we study the effect of  $t, d$  on the behavior of  $T_c$ . First, we focus on the  $T_c$  behavior at unitarity as a function of  $t$  and  $d$ , since the unitary limit is a special point where the scattering length diverges, and thus the system may exhibit some universal behaviors.

Shown in Fig. 3 are log-log plots of  $T_c$  as a function of (a)  $d$  and (b)  $t$ , respectively. Their linear plots are given in the corresponding insets. Here we treat  $t$  and  $d$  as independent parameters, so that they may enter the experimentally inaccessible regime. Panel (a) covers a broad range of the  $(t, d)$  parameter space, from large  $t = 0.5E_F$  to small  $t = 0.05E_F$ , and from tiny  $k_F d = 0.0001$  to large  $k_F d = 10$ . Surprisingly,  $T_c$  exhibits a very good power law across such a big parameter space, with a scaling  $T_c \propto d^\alpha$ , where  $\alpha$  is close to 0.655 for small  $d$  and 0.59 for large  $d$ . Similarly, panel (b) also covers from  $k_F d = 1$  to 8, and from  $t/E_F = 0.0001$  to 1.0, and  $T_c$  scales as  $T_c \sim t^\beta$ , where  $\beta = 0.445$  for small  $t$  and 0.41 for large  $t$ . Overall, at unitarity, we have

$$T_c \sim d^\alpha t^\beta, \quad \alpha = 0.59 \sim 0.655, \quad \beta = 0.41 \sim 0.445. \quad (15)$$

Next, we show in Fig. 4 the  $T_c$  curves throughout the entire BCS-BEC crossover as a function of  $1/k_F a$  for different  $t$  and  $d$ . Shown in panels (a) and (b) is  $T_c$  for fixed  $t/E_F = 0.2$  and 0.01, respectively, but with different values of  $d$ . Here we keep the product  $td^2 < 1/2m$ . As we can see, for fixed  $t$ , the maximum  $T_c$ ,  $T_c^{\max}$ , increases with increasing  $d$ . At the same time, the entire  $T_c$  curve is compressed horizontally toward unitarity, as  $d$  increases. This is in accord with the exponential behavior of  $\mu \sim -e^{d/a}$  in the BEC regime. We plot  $T_c^{\max}$  versus  $d$  in the corresponding insets, which exhibits a quasilinear behavior. The comparison between Figs. 4(a) and 4(b) for the same  $d$  reveals that  $T_c$  increases with  $t$ . Indeed,  $T_c$  will be suppressed logarithmically to zero as  $t$  approaches 0 [15]. We also note that the peak of maximum  $T_c$  moves away from unitarity toward the BEC side as  $d$  decreases. This also has to do with the exponential behavior of  $\mu \sim -e^{d/a}$ .

In Fig. 4(c), we present the  $T_c$  curves for fixed  $2mt d^2 = 0.2$  while changing  $k_F d$  from 0.5 to 10. Since  $t$  decreases as  $d$  increases, it is not surprising to see nonmonotonic behavior of

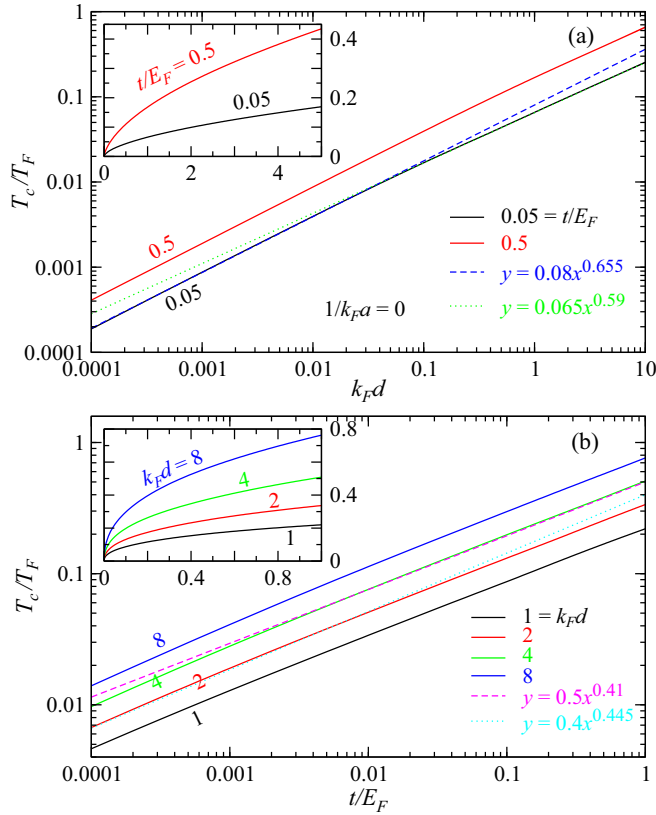


FIG. 3. Behavior of  $T_c$  at unitarity as a function of (a)  $k_F d$  with  $t/E_F = 0.05$  (black solid lines) and  $0.5$  (red lines) and of (b)  $t/E_F$  with  $k_F d = 1$  (black),  $2$  (red),  $4$  (green), and  $8$  (blue solid lines), respectively, as labeled. Also shown in (a) are simple power laws, which fit the small (blue dashed) and large (green dotted)  $d$  ranges well, respectively. Similarly, the cyan dashed and magenta dotted lines in (b) are simple power laws which fit the  $T_c$  curves well in the large and small  $t$  regimes, respectively.

$T_c^{\max}$  versus  $d$ , as shown in the inset. Nonetheless, we still see an overall increase of  $T_c^{\max}$  with  $d$  while keeping  $td^2$  fixed. This increase is not as dramatic as the fixed  $t$  cases, reflecting the competing effects between increasing  $d$  and decreasing  $t$ .

It should be pointed out that the increase of  $T_c$  in Fig. 4 will disappear if we use the respective Fermi level  $\mu_0$  in the noninteracting limit as the energy unit, as  $\mu_0$  increases with  $t$  and  $d$  as well [46]. Nevertheless, this increase does make sense when one compares  $T_c$  with the 3D homogeneous system of the same fermion density.

With multiple tunable parameters, the complete superfluid phase diagram is very complex, occupying a hyper volume in the high-dimensional phase space. We can show only hypersurfaces corresponding certain fixed parameters. As an example, presented in Fig. 5 are  $T_c$  contours in the  $k_F d - 1/k_F a$  plane with fixed  $t/E_F = 0.1$ . The range of  $d$  is restricted roughly within  $2md^2 < 1$ . From this figure, one can see that the highest  $T_c \gtrsim 0.15$  is achieved at large  $d$  near unitarity. The higher concentration of curves at large  $d$  indicates that the  $T_c$  curve is highly compressed toward unitarity as  $d$  increases, as shown in Fig. 4. On the contrary, when  $d$  becomes small ( $\ll 1$ ), the  $T_c$  curve as a function of  $1/k_F a$  will be suppressed down and expanded along the  $1/k_F a$  axis. One can also consider

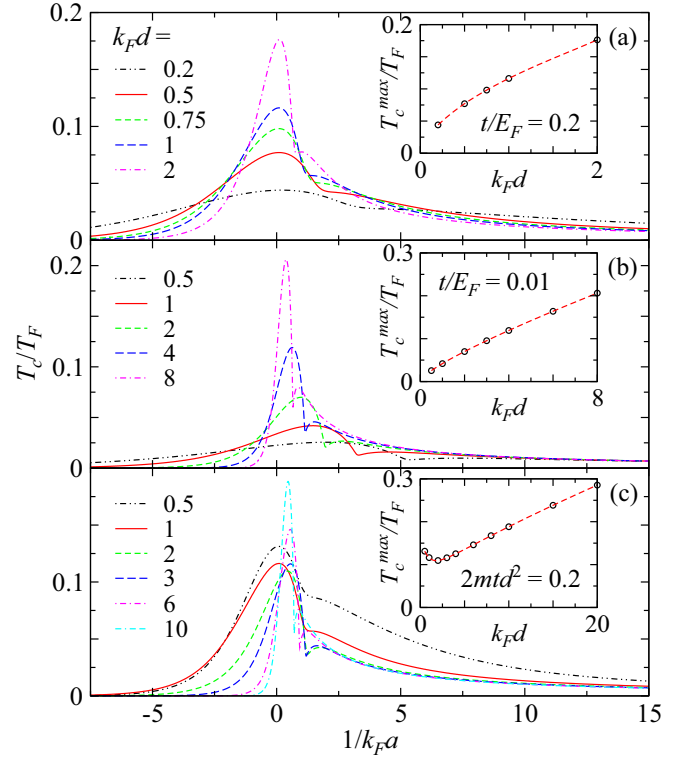


FIG. 4.  $T_c$  curves as a function of  $1/k_F a$  for different values of  $k_F d$  at fixed (a)  $t/E_F = 0.2$ , (b)  $0.01$ , and (c)  $2md^2 = 0.2$ . The maximum  $T_c$  near unitarity,  $T_c^{\max}$ , as a function of  $d$ , is plotted in the respective inset.

a vertical cut at fixed  $1/k_F a$  in Fig. 5. A cut at  $1/k_F a = 0$  will yield a curve as in the inset of Figs. 4(a) and 4(b). The peak/dip structure of the  $T_c$  contours at positive  $1/k_F a$  for  $k_F d = 0.03 \sim 0.07$  in Fig. 5 is associated with the dip near  $\mu = 0$  in the  $T_c$  versus  $1/k_F a$  curves, as shown in Fig. 4. Another feature that is worth mentioning is the small kink in the contours on the BCS side, especially for the lowest

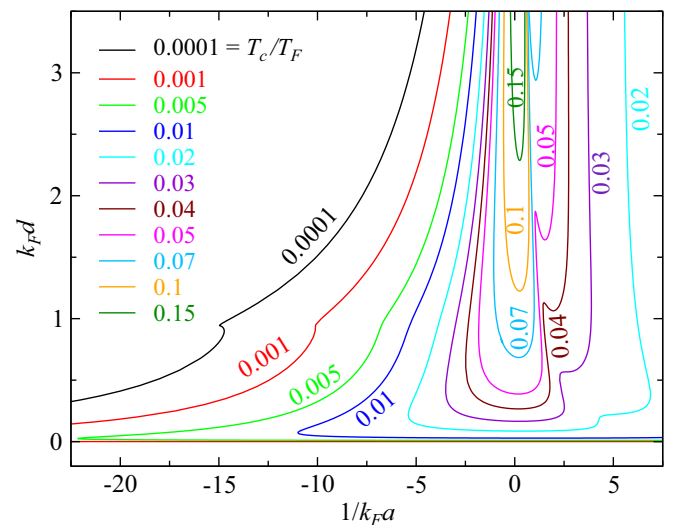


FIG. 5. Contour plot of  $T_c/T_F$  in the  $k_F d - 1/k_F a$  plane for fixed  $t/E_F = 0.1$ . The corresponding  $T_c$  values are labeled near the curves.

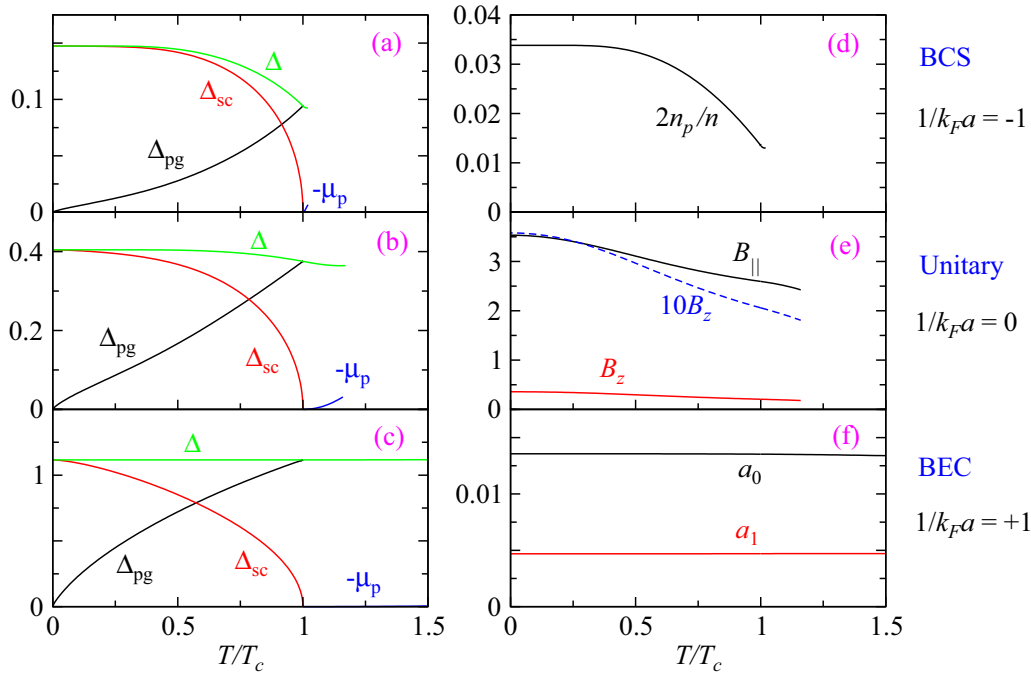


FIG. 6. Behavior of the gaps and  $-\mu_p$ , as labeled, as a function of  $T/T_c$ , for (a)  $1/k_F a = -1$ , (b) 0, (c)  $+1$ , with  $T_c/T_F = 0.07060, 0.13135,$  and  $0.05156$ , for the BCS, unitary, and BEC regimes, respectively. Also plotted are (d)  $2n_p/n$  for  $1/k_F a = -1$ , (e)  $B_{||}$  and  $B_z$  as well as  $10B_z$  for  $1/k_F a = 0$ , and (f)  $a_0$  and  $a_1$  for  $1/k_F a = +1$ . Here  $t/E_F = 0.1$ , and  $k_F d = 2$ . Gaps and chemical potential are in units of  $E_F$ . The coefficients  $B$ 's are in units of  $1/2m$ ,  $a_0$  and  $a_1$  in units of  $k_F^3/E_F^2$  and  $k_F^3/E_F^3$ , respectively.

$T_c/T_F = 0.0001$ . As can be seen, for all contours, this kink happens slightly below  $k_F d = 1$ . For  $t/E_F = 0.1$ , the topology of the Fermi surface changes from open to closed at  $k_F d \approx 0.945$ . The van Hove singularity associated with this topological change leads to logarithmic divergence of the density of states at the Fermi level, and thus significantly enhances  $T_c$ , so that the  $T_c$  contour will deform toward weaker pairing strength, as indeed shown by the low  $T_c$  contours in Fig. 5. This singularity effect is washed out gradually by thermal broadening as  $T$  increases. It becomes barely noticeable for  $T_c/T_F \geq 0.01$ . Note that the van Hove singularity effect on  $T_c$  cannot readily be seen in other types of plot.

### B. Gaps in the superfluid phase

In Fig. 6, we present, as an example, the behavior of the order parameter  $\Delta_{sc}$  (red), the pseudogap  $\Delta_{pg}$  (black), and the total gap  $\Delta$  (green curves) and a few relevant quantities as a function of temperature in the superfluid phase. Also plotted is the solution slightly above  $T_c$ , especially for the pair chemical potential  $\mu_p$ . Shown in the figure is for the case of  $k_F d = 2$ ,  $t/E_F = 0.1$  for  $1/k_F a = -1, 0,$  and  $+1$ , for the BCS, unitary, and BEC regimes, respectively. There exists a pseudogap in all cases throughout the BCS–BEC crossover, as in the regular 3D continuum case [43]. The order parameter  $\Delta_{sc}$  sets in at  $T_c$  with decreasing  $T$ , while the pseudogap  $\Delta_{pg}$  starts to decrease. The total gap increases with decreasing  $T$  in the BCS regime, where  $\Delta_{pg}$  is small, but stays roughly constant for the unitary and BEC cases. Above  $T_c$ , the pair chemical potential  $\mu_p$  starts to decrease from 0 with increasing  $T$ . As seen in the figure,  $-\mu_p$  increases much faster in the BCS than in the BEC regimes as a function of  $T$  above  $T_c$ . This makes our simplified

BCS form of the pseudogap self energy become quickly less accurate above  $T_c$  in the BCS regime. The curves stop roughly where the approximation becomes inaccurate.

Figure 6(a) suggests that  $-\mu_p$  increases linearly with  $(T - T_c)$ . Indeed, as one often finds in the weak fluctuation treatment in the framework of the mean-field BCS theory,  $\mu_p \propto -(T - T_c)$  above  $T_c$  in the BCS limit [47,48]. As the pairing becomes stronger,  $\mu_p$  becomes quadratic in  $(T - T_c)$ , as manifested in Fig. 6(b). For the BEC case in Fig. 6(c),  $-\mu_p$  stays small up to very high  $T \gg T_c$ . In this case, the gaps are large, and essentially all atoms form pairs, so that the system exhibits behaviors that are close to an ideal Bose gas.

We show in Fig. 6(d) the pair fraction for the BCS case, where the pairing is weak and the pair fraction is small. The temperature dependence of  $n_p$  follows roughly that of  $\Delta^2$  via Eq. (5), as  $a_0$  is less sensitive to  $T$ . The pair density  $n_p$  increases with  $1/k_F a$  and becomes  $n/2$  for  $1/k_F a = +1$ , which has  $\mu/E_F \approx -0.12 < 0$  for all  $T \leq T_c$ . For  $B_{||}$  and  $B_z$ , we show for the unitary case in Fig. 6(e). Their temperature dependencies are stronger in the BCS regime and weaker in the BEC regime. In addition,  $B_{||}$  approaches  $1/4m$  in the BEC limit. At the same time,  $B_z$  becomes exponentially smaller in the BEC regime, as given by Eq. (10). Finally, the  $T$  dependencies of  $a_0$  and  $a_1$  are shown in Fig. 6(f) for the BEC case. Both  $a_0$  and  $a_1$  become essentially  $T$  independent, as does the total gap. It is also evident that  $a_1 T_c \ll a_0$  for this case. The  $a_1$  term in the inverse  $T$ -matrix expansion is quantitatively important only in the BCS regime, where we find  $a_1 T_c/a_0 \sim 10$  for the case in Fig. 6(a). More detailed discussions of the influence of the  $a_1$  term can be found in Ref. [44] for the somewhat similar 3D continuum case.

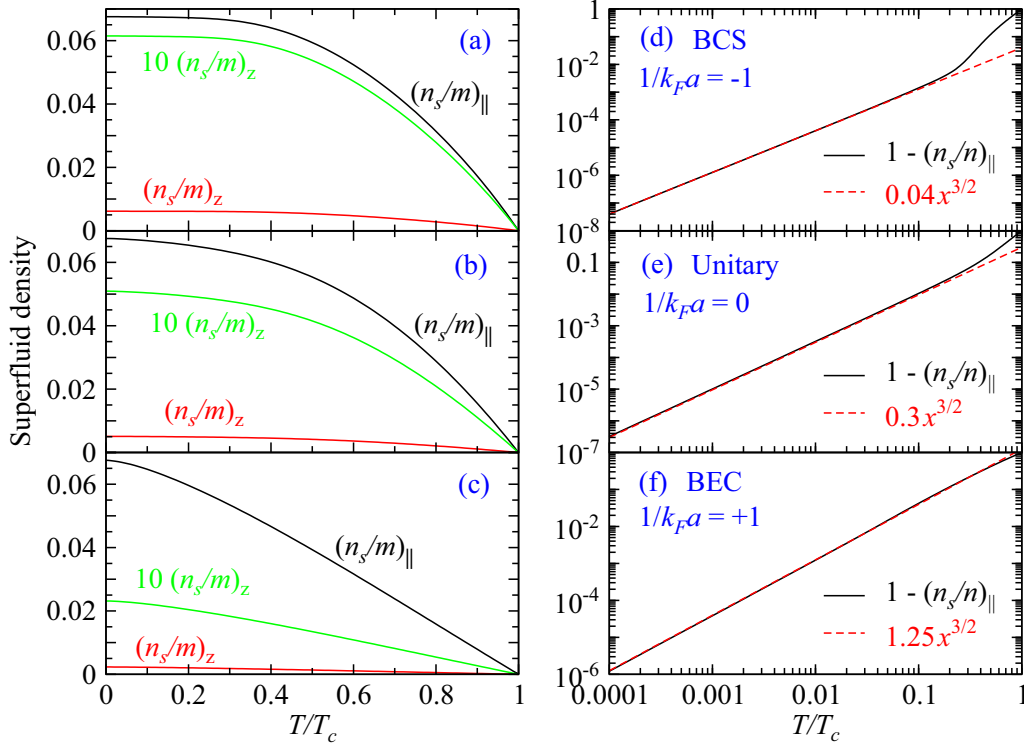


FIG. 7. Behavior of the in-plane (black curves) and lattice components (red curves) of the superfluid densities, as labeled, as a function of  $T/T_c$ , for (a)  $1/k_F a = -1$ , (b) 0, (c)  $+1$ , for the BCS, unitary, and BEC regimes, respectively, corresponding to Fig. 6. Also shown is  $10(n_s/m)_z$  (green curves) for clarity. Plotted in (d-f) are the corresponding normal fluid fraction  $1 - (n_s/n)_\parallel$  (black solid curves) in log-log scales, and simple  $T^{3/2}$  power laws (red dashed lines) for comparison. The zero  $T$  value of  $(n_s/m)_\parallel$  is given by  $2/3\pi^2$  in our convention of units.

### C. Superfluid density

Now we present the result for the superfluid density calculations. Shown in Fig. 7 are the in-plane and lattice components of the superfluid density, from top to bottom, for the BCS, unitary and BEC cases (of Fig. 6), respectively. The left column presents  $(n_s/m)_\parallel$  (black) and  $(n_s/m)_z$  (red), as well as  $10(n_s/m)_z$  (green curves). The right column presents the in-plane normal fluid fraction,  $1 - (n_s/n)_\parallel$ , as a function of  $T/T_c$  in log-log scales (black solid lines). For comparison, we plot simple power laws of  $(T/T_c)^{3/2}$  (red dashed lines), with different coefficients to fit roughly the corresponding solid lines. Here the message is clear. In the BCS case, the linear plot in Fig. 7(a) looks very much like an exponential  $T$  dependence at low  $T$ . Only a log-log plot in Fig. 7(d) reveals that the leading dominant term is actually a  $T^{3/2}$  power law. The small coefficient, 0.04, in front of  $(T/T_c)^{3/2}$ , is consistent with the flatness of  $(n_s/m)_\parallel$  at low  $T$  in Fig. 7(a). Nevertheless, the power-law contributions from finite momentum pairs always dominate the exponentially activated term from Bogoliubov quasiparticles. As the pairing strength, or  $1/k_F a$ , increases, the magnitude of the power law term becomes larger. For the unitary case, even in the linear plot in Fig. 7(b),  $(n_s/m)_\parallel$  deviates strongly from exponential behavior. The coefficient increases to 0.3, as shown in Fig. 7(e). For the BEC case in Fig. 7(c), the quasiparticle contributions become negligible, and  $(n_s/m)_\parallel$  becomes almost purely a  $(T/T_c)^{3/2}$  power law. As one can see in Fig. 7(f), the dash line overlays with the solid curve essentially for the entire range of

$T \leq T_c$ . It should be noted, however, that the coefficient is now 1.25, larger than 1. This reflects the fact that the system is quasi-2D rather than 3D; a pure  $(T/T_c)^{3/2}$  is only for a pure 3D case. Indeed, as one can see from Fig. 7(c),  $(n_s/m)_\parallel$  becomes more of a straight line for the upper half of  $T/T_c$ , to be compatible with the larger-than-unity coefficient 1.25. Theoretically, as  $T$  becomes higher, more high in-plane momentum  $q_\parallel$  pairs will be excited, which can feel the quasi-two dimensionality.

The lattice component of the superfluid density,  $(n_s/m)_z$ , (red curves) in Figs. 7(a)–7(c) is substantially smaller than  $(n_s/m)_\parallel$ , as discussed earlier. Its temperature dependence is close to that of  $(n_s/m)_\parallel$ , as can be seen more clearly from the (green)  $10\times$  magnified curves. This is because both are mainly governed by the prefactor  $\Delta_{sc}^2 = \Delta^2 - \Delta_{pg}^2$  in Eq. (14), and the second term,  $\Delta_{pg}^2 \propto T^{3/2}$ , yields the  $T^{3/2}$  power law for both components of  $(n_s/m)$ . For the present  $s$ -wave pairing, the rest of Eq. (14) yields an exponential  $T$  dependence for the normal fluid,  $e^{-\Delta/T}$ , and thus becomes negligible at low  $T$ . It is also evident that  $(n_s/m)_z$  decreases as the pairing becomes stronger toward BEC. This can be understood since  $v_k^2$  becomes more widespread in momentum space as  $1/k_F a$  increases, and thus pairs feel more strongly the effect of lattice momentum cutoff in the  $z$  direction, so that the system becomes effectively more 2D. At the same time the mobility of the pairs is controlled by  $t_B$ , which decreases rapidly with  $1/k_F a$ . This determines the magnitude of  $(n_s/m)_z$  in the BEC regime.

**IV. CONCLUSIONS**

In summary, we have studied the ultracold atomic Fermi gases in a 1D optical lattice with a pairing fluctuation theory, as they undergo a BCS-BEC crossover. We find that  $T_c$  decreases with  $1/k_F a$  in the BEC regime and approaches asymptotically  $T_c/T_F = \pi a n/2m$ , which is independent of the lattice parameters  $t$  and  $d$ . Both  $|\mu|$  and the gap  $\Delta$  grow exponentially as  $e^{d/a}$  and  $e^{d/2a}$ , respectively, in the BEC regime so that the pair hopping integral  $t_B$  decreases as  $e^{-d/a}$ . Moreover, the (maximum)  $T_c$  near unitarity increases with both  $t$  and  $d$ , with fractional power-law exponents. On the BCS side, the effect of van Hove singularity on  $T_c$  has been identified in the  $T_c$  contours.

We find generally a pseudogap above and below  $T_c$ , away from the extreme BCS limit. While the total gap  $\Delta$  is a smooth function across  $T_c$ , the order parameter sets in at  $T_c$ , and the pseudogap starts to decrease as  $T$  decreases below  $T_c$ . Our calculated behavior of the pair chemical potential  $\mu_p$  above  $T_c$  are also in good agreement with existing literature. At low  $T$ ,  $\Delta_{pg}^2 \sim T^{3/2}$ . This leads to  $T^{3/2}$  power laws for the low  $T$  dependence of the superfluid density, despite that it looks visually like exponential in the BCS regime.

While there is not yet a generic simple formula to relate the parameter  $a$  with its 3D continuum counterpart  $a_{3D}$ , experimentally one can use the chemical potential  $\mu$  as a control parameter to uniquely locate where the system is, just as has been done using the binding energy  $\epsilon_B$  for Fermi gases in a tightly confined 2D trap.

Our findings have not been reported in the literature. Although precise control and measurements of the gaps and superfluid density remains challenging experimentally at present, we believe that our predictions can be tested in future experiments.

**ACKNOWLEDGMENTS**

We thank Chenchao Xu, Lin Sun, and Yanming Che for useful discussions. This work was supported by the NSF of China (Grants No. 11774309 and No. 11674283), and the NSF of Zhejiang Province of China (Grant No. LZ13A040001). C.L. was supported by the Key-Area Research and Development Program of Guangdong Province under Grant No. 2019B030330001, the NSF of China under Grants No. 11874434 and No. 11574405, and the Science and Technology Program of Guangzhou (China) under Grant No. 201904020024.

**APPENDIX A: EVOLUTION OF  $1/k_F a$  VERSUS  $t$  AND ITS CONNECTION TO THE 2D LIMIT**

To regularize the ultraviolet divergence in the integral of the gap equation caused by the contact potential, we have introduced a scattering length  $a$ , via the Lippmann-Schwinger relation,

$$\frac{m}{4\pi a} = \frac{1}{U} + \sum_{\mathbf{k}} \frac{1}{2\epsilon_{\mathbf{k}}}. \tag{A1}$$

Due to the restricted momentum space in the lattice direction, this definition is similar to but different from its counterpart

in isotropic 3D free space. In this definition, the anisotropy of the (effective) fermion mass was not considered. Needless to say, this scattering length parameter does not correspond to the actual scattering length when measured experimentally. Nonetheless, it can be regarded as an effective parameter for characterizing the interaction strength, just as in 3D continuum.

In the  $t \rightarrow 0$  limit, where the system becomes 2D, this scattering length is rather different from the physical 2D  $s$ -wave scattering length,  $a_{2D}$ , which is given by

$$\epsilon_B = \frac{\hbar^2}{ma_{2D}^2}, \tag{A2}$$

where  $\epsilon_B$  is the two-body binding energy. In the BEC regime,  $\epsilon_B \approx -2\mu$ . It should be noted, however, that  $a_{2D}$  is always positive and diverges in the zero pairing strength limit, since an arbitrarily weak attractive interaction (including those of a finite range) is enough to form bound state in vacuum. Meanwhile, besides the ultraviolet divergence, infrared divergence also emerges in the momentum integral in the pair susceptibility  $\chi(0)$  in exact 2D, as  $t \rightarrow 0$ . In exact 2D, the gap equation is regularized in a different way, via [49,50]

$$\frac{1}{U} = - \sum_{\mathbf{k}} \frac{1}{\epsilon_B + 2\epsilon_{\mathbf{k}}}, \tag{A3}$$

which relates  $1/U$  with  $a_{2D}$ . Since there is a logarithmic energy dependence in the low energy  $s$ -wave scattering phase shift, there is no easy way to define a single scattering length parameter which evolves continuously from 3D to 2D.

From Eq. (A1), it is clear that the infrared divergence at  $t = 0$  leads to a logarithmic dependence of  $1/a$  on  $t$ . Indeed, from Eq. (7) in the main text, we obtain in the BEC regime,

$$\frac{1}{a} \approx \frac{1}{d} \ln \frac{|\mu|}{t} = -\frac{1}{d} \ln (2mta_{2D}^2). \tag{A4}$$

We have checked Eq. (A4) numerically by solving our set of equations with fixed  $\mu$  as a function of  $t$ . Shown in Fig. 8 is  $1/k_F a$  as a function of  $t/E_F$  in a semilog scale, calculated for  $d = 2$  with  $\mu/E_F = -10$  at low  $T$  ( $T_c$  to be precise). The perfect straight line fully verifies the logarithmic dependence

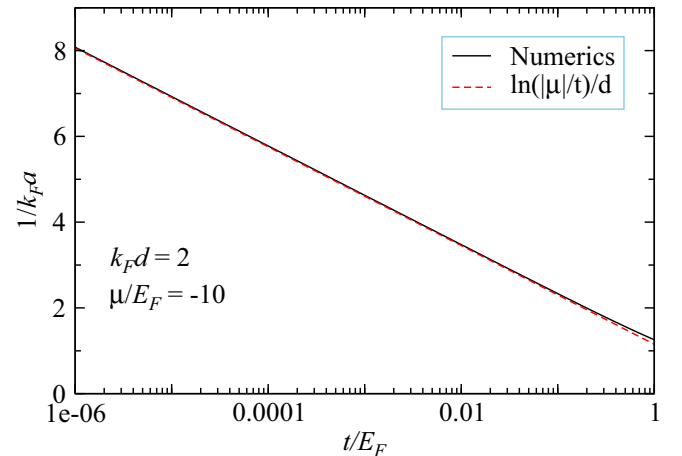


FIG. 8. Behavior of  $1/k_F a$  as functions of  $t/E_F$  in the BEC regime at fixed  $\mu/E_F = -10$  for  $k_F d = 2$ .

given in Eq. (A4). Also shown is the analytical expression of Eq. (A4) (red dashed line), which overlays on top of the numerical solution except for the slight difference at large  $t$ , where the correction terms in Eq. (7) in the main text becomes quantitatively significant.

One should not be misled by Eq. (7) to think that the term  $-te^{d/a}$  vanishes in the BEC limit as  $t \rightarrow 0$ . Instead, for a given binding energy in the 2D limit, our  $1/k_F a$  diverges logarithmically following Eq. (A4). Moreover, for a fixed  $1/k_F a$ ,  $\mu$  approaches its noninteracting 2D value,  $\pi dn/m$ , as  $t \rightarrow 0$ , as we have verified numerically.

In this quasi-2D regime, the dispersion in the lattice dimension mainly serves as an infrared cutoff for the momentum integral in the gap equation. One can essentially neglect the pairing in this direction and assuming the in-plane pairing interaction  $U$  is the same as that in the absence of the lattice,  $U_{3D}$ . Now one can relate the present scattering length parameter  $a$  with its 3D counterpart  $a_{3D}$  by canceling out the pairing interaction via the Lippmann-Schwinger equations and obtain

$$\frac{m}{4\pi a} - \frac{m}{4\pi a_{3D}} = \alpha - \alpha_{3D} \equiv \sum_{\mathbf{k}} \frac{1}{2\epsilon_{\mathbf{k}}} - \sum_{\mathbf{k}} \frac{1}{2\epsilon_{\mathbf{k}}^{3D}}, \quad (\text{A5})$$

where  $\epsilon_{\mathbf{k}}^{3D} = k^2/2m$  is the free dispersion in 3D. Also note that the integration of the lattice dimension in  $\alpha$ , i.e., the first integral on the right-hand side (rhs) of the equation, is restricted to the first BZ while there is no such restriction for the second integral for  $\alpha_{3D}$ . It is obvious that the two terms on the rhs have ultraviolet divergences logarithmic and linear in  $k$ , respectively, and they do not cancel each other. A concrete momentum cutoff  $k_0$  that is true to the physical system is necessary, and one cannot take the unphysical contact limit for the pairing potential. When  $t$  is small and  $d$  is small, the integral over  $k_z$  in  $\alpha$  leads to a factor of  $1/d$ , which is similar to the result for  $a_{2D}$  for a tightly confined 2D trap [51]. For fixed  $k_0$ ,  $\alpha_{3D}$  becomes negligible when  $d$  becomes very small. For a box cutoff with  $k_0 = 100k_F$  and  $t/E_F = 0.01$ , the expression of Eq. (A5) is plotted in Fig. 9, as a function of  $k_F d$ , which exhibits a  $1/d$  divergence as a function of  $d$ . An extra logarithmic infrared divergence kicks in as  $t$  approaches

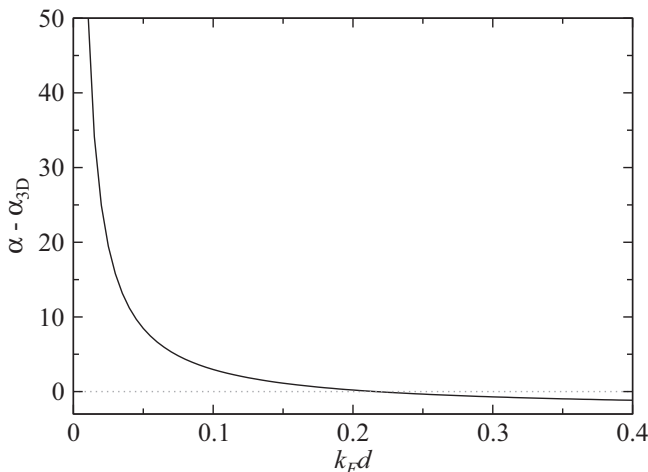


FIG. 9. Behavior of  $\alpha - \alpha_{3D}$  as functions of  $k_F d$  for  $t/E_F = 0.01$  and  $k_0/k_F = 100$ .

0. In these cases,  $1/a$  will diverge, in agreement with Eq. (A4), and thus the use of  $a_{2D}$  as defined in Eqs. (A2)–(A4) becomes more appropriate.

It should be noted, however, that the relationship between  $a$  and  $a_{3D}$  in Eq. (A5) may not be valid beyond the quasi-2D regime. As the cutoff  $k_0$  increases to approach the contact limit, the critical coupling strength  $U_c$  for two atoms to form a bound state will necessarily be renormalized down to zero. This is obviously incorrect for the lattice dimension, as it means the pairing interaction in the lattice direction will vanish.

In fact, the scattering length in cold atoms is tuned via the Feshbach mechanism, which relies on the two-channel model, with both open-channel atomic scattering states and closed-channel molecular bosons [4,52]. The overall effective interaction comes from contributions of both channels. In the presence of a lattice potential, the bare propagator of the closed channel bosons is modified, and hence so is their contribution to the overall pairing interaction. It remains a question as to how the pairing interaction behaves when a lattice potential is turned on.

Despite that one does not have a general simple relation between  $a$  and  $a_{3D}$  for arbitrary  $t$  and  $d$ , one can use the experimentally measured chemical potential  $\mu$  as a control variable to locate where the system is in the phase diagram, just as one does for a Fermi gas in a single 2D trap, (where  $\mu$  is replaced by  $\epsilon_B$ ).

## APPENDIX B: EFFECTIVE SCATTERING LENGTH $a_{\text{eff}}$

The strong  $t$  (and  $d$ ) dependence of  $a$  defined via Eq. (A1) suggests that the parameter  $a$  is not comparable to the physical scattering length. Here we try to define an effective scattering length  $a_{\text{eff}}$ , which more or less reflects the physical scattering length.

Consider the long wave length limit of dispersion  $\epsilon_{\mathbf{k}}$ , and rescale  $k_z$  such that  $k'_z = \sqrt{2mtd}k_z$ . Then for small  $\mathbf{k}' \equiv (k_x, k_y, k'_z)$ , we have

$$\epsilon_{\mathbf{k}'} = \frac{1}{2m}(\mathbf{k}'_{\parallel}{}^2 + k'_z{}^2), \quad (\text{B1})$$

which is isotropic in  $\mathbf{k}'$ . In this way,  $\sum_{\mathbf{k}}$  becomes  $\frac{1}{\sqrt{2mtd}} \sum_{\mathbf{k}'}$ . Then the Lippmann-Schwinger equation becomes

$$\frac{m}{4\pi a_{\text{eff}}} \equiv \frac{m}{4\pi a} \sqrt{2mtd} = \frac{1}{U'} + \sum_{\mathbf{k}'} \frac{1}{2\epsilon_{\mathbf{k}'}}, \quad (\text{B2})$$

where  $U' = U/\sqrt{2mtd}$  is the rescaled interaction. Comparing this equation to the Lippmann-Schwinger equation in 3D free space, we expect the quantity

$$a_{\text{eff}} = \frac{a}{\sqrt{2mtd}} \quad (\text{B3})$$

to be comparable to the 3D scattering length  $a_{3D}$  used in experiment. Indeed, as one can see from Fig. 1 of Ref. [53] that, the horizontal axis scale of the  $p - 1/k_F a$  phase diagram, when plotted using  $1/k_F a_{\text{eff}}$ , closely matches that of a 3D continuum case in Ref. [54].

From Eqs. (A4) and (B3), we obtain the relationship between  $a_{2D}$  and  $a_{\text{eff}}$  as

$$a_{2D} = \frac{1}{\sqrt{2mt}} e^{-d/2a} = \frac{1}{\sqrt{2mt}} e^{-1/2\sqrt{2mt}a_{\text{eff}}}, \quad (\text{B4})$$

which resembles closely the relationship between  $a_{2D}$  and  $a_{3D}$  for a tightly confined quasi-2D atomic gas [51], with  $1/\sqrt{2mt}$  playing the role of oscillator length.

Finally, it should be mentioned that, despite that it can characterize the interaction strength,  $a_{3D}$  is not the actual physical scattering length, either, since it is defined in the absence of the optical lattice potential.

### APPENDIX C: COEFFICIENTS OF THE TAYLOR-EXPANDED INVERSE $T$ -MATRIX

In this Appendix, we present concrete expressions for the coefficients of the Taylor expansion of the inverse  $T$ -matrix,  $t(\Omega, \mathbf{q})$ , after analytical continuation,

$$t_{\text{pg}}^{-1}(\mathbf{q}, \Omega) = a_1 \Omega^2 + a_0(\Omega - \Omega_{\mathbf{q}} + \mu_{\text{p}} + i\Gamma_{\mathbf{q},\Omega}). \quad (\text{C1})$$

Here  $\mu_{\text{p}} = t^{-1}(0, 0)/a_0$ , which vanishes for  $T \leq T_c$ . In the long wavelength limit,

$$\Omega_{\mathbf{q}} = B_{\parallel} q_{\parallel}^2 + B_z q_z^2 \equiv \frac{q_{\parallel}^2}{2M_{\parallel}} + \frac{q_z^2}{2M_z}, \quad (\text{C2})$$

with  $B_z = t_{\text{B}} d^2$ .

Before expansion, the inverse  $T$  matrix is given by

$$t_{\mathbf{q},\Omega+i0^+}^{-1} = U^{-1} + \sum_{\mathbf{k}} \left[ \frac{1 - f(E_{\mathbf{k}}) - f(\xi_{\mathbf{k}-\mathbf{q}})}{E_{\mathbf{k}} + \xi_{\mathbf{k}-\mathbf{q}} - \Omega - i0^+} u_{\mathbf{k}}^2 - \frac{f(E_{\mathbf{k}}) - f(\xi_{\mathbf{k}-\mathbf{q}})}{E_{\mathbf{k}} - \xi_{\mathbf{k}-\mathbf{q}} + \Omega + i0^+} v_{\mathbf{k}}^2 \right]. \quad (\text{C3})$$

Then we have

$$\begin{aligned} a_0 &= \frac{1}{2\Delta^2} \sum_{\mathbf{k}} \left\{ [1 - 2f(\xi_{\mathbf{k}})] - \frac{\xi_{\mathbf{k}}}{E_{\mathbf{k}}} [1 - 2f(E_{\mathbf{k}})] \right\} \\ &= \frac{1}{2\Delta^2} \left[ n - 2 \sum_{\mathbf{k}} f(\xi_{\mathbf{k}}) \right], \end{aligned} \quad (\text{C4})$$

$$\begin{aligned} a_1 &= \frac{1}{2\Delta^4} \sum_{\mathbf{k}} E_{\mathbf{k}} \left\{ \left( 1 + \frac{\xi_{\mathbf{k}}^2}{E_{\mathbf{k}}^2} \right) [1 - 2f(E_{\mathbf{k}})] \right. \\ &\quad \left. - 2 \frac{\xi_{\mathbf{k}}}{E_{\mathbf{k}}} [1 - 2f(\xi_{\mathbf{k}})] \right\}, \end{aligned} \quad (\text{C5})$$

and the imaginary part

$$\begin{aligned} \Gamma_{\mathbf{q},\Omega} &= \frac{\pi}{a_0} \sum_{\mathbf{k}} \left\{ [1 - f(E_{\mathbf{k}}) - f(\xi_{\mathbf{k}-\mathbf{q}})] u_{\mathbf{k}}^2 \delta(E_{\mathbf{k}} + \xi_{\mathbf{k}-\mathbf{q}} - \Omega) \right. \\ &\quad \left. + [f(E_{\mathbf{k}}) - f(\xi_{\mathbf{k}-\mathbf{q}})] v_{\mathbf{k}}^2 \delta(E_{\mathbf{k}} - \xi_{\mathbf{k}-\mathbf{q}} + \Omega) \right\}. \end{aligned} \quad (\text{C6})$$

We have  $\Gamma_{\mathbf{q},\Omega} = 0$  when  $-(E_{\mathbf{k}} - \xi_{\mathbf{k}-\mathbf{q}})_{\text{min}} < \Omega_{\mathbf{q}} < (E_{\mathbf{k}} + \xi_{\mathbf{k}-\mathbf{q}})_{\text{min}}$ , and in general  $\Gamma_{\mathbf{q},\Omega}$  is much smaller than  $\Omega_{\mathbf{q}}$  for small  $q$  at  $T \leq T_c$ . For details, see Ref. [44].

The pair dispersion coefficients are given by

$$\begin{aligned} B_i &= \frac{1}{2} \frac{\partial^2 \Omega_{\mathbf{q}}}{\partial q_i^2} \Big|_{\mathbf{q}=0} \\ &= -\frac{1}{2a_0 \Delta^2} \sum_{\mathbf{k}} \left[ \left( 2f'(\xi_{\mathbf{k}}) + \frac{E_{\mathbf{k}}}{\Delta^2} \left\{ \left( 1 + \frac{\xi_{\mathbf{k}}^2}{E_{\mathbf{k}}^2} \right) [1 - 2f(E_{\mathbf{k}})] \right. \right. \right. \\ &\quad \left. \left. - 2 \frac{\xi_{\mathbf{k}}}{E_{\mathbf{k}}} [1 - 2f(\xi_{\mathbf{k}})] \right\} \right) \left( \frac{\partial \xi_{\mathbf{k}}}{\partial k_i} \right)^2 \\ &\quad \left. - \frac{1}{2} \left\{ [1 - 2f(\xi_{\mathbf{k}})] - \frac{\xi_{\mathbf{k}}}{E_{\mathbf{k}}} [1 - 2f(E_{\mathbf{k}})] \right\} \frac{\partial^2 \xi_{\mathbf{k}}}{\partial k_i^2} \right]. \end{aligned} \quad (\text{C7})$$

Given the dispersion  $\xi_{\mathbf{k}} = \frac{k_{\parallel}^2}{2m} - 2t[1 - \cos(k_z d)] - \mu$  for 1DOL, we have, for  $i = x, y$ ,

$$\left( \frac{\partial \xi_{\mathbf{k}}}{\partial k_i} \right)^2 = \frac{k_i^2}{m^2}, \quad \frac{\partial^2 \xi_{\mathbf{k}}}{\partial k_i^2} = \frac{1}{m},$$

and for  $i = z$ ,

$$\left( \frac{\partial \xi_{\mathbf{k}}}{\partial k_z} \right)^2 = (2td)^2 \sin^2(k_z d), \quad \frac{\partial^2 \xi_{\mathbf{k}}}{\partial k_z^2} = 2td^2 \cos(k_z d).$$

- 
- [1] M. Köhl, H. Moritz, T. Stöferle, K. Günter, and T. Esslinger, Fermionic Atoms in a Three-Dimensional Optical Lattice: Observing Fermi Surfaces, Dynamics, and Interactions, *Phys. Rev. Lett.* **94**, 080403 (2005).
- [2] I. Bloch, Ultracold quantum gases in optical lattices, *Nat. Phys.* **1**, 23 (2005).
- [3] A. Georges, Condensed matter physics with light and atoms: Strongly correlated cold fermions in optical lattices, in *Ultracold Fermi Gases*, in *Proceedings of the International School of Physics "Enrico Fermi", Vol. CLXIV*, edited by M. Inguscio, W. Ketterle, and C. Salomon, *Società Italiana di Fisica Bologna, Italy* (IOS Press, Amsterdam, 2008), pp. 477–510.
- [4] Q. J. Chen, J. Stajic, S. N. Tan, and K. Levin, BCS-BEC crossover: From high temperature superconductors to ultracold superfluids, *Phys. Rep.* **412**, 1 (2005).
- [5] I. Bloch, J. Dalibard, and W. Zwerger, Many-body physics with ultracold gases, *Rev. Mod. Phys.* **80**, 885 (2008).
- [6] S. Giorgini, L. P. Pitaevskii, and S. Stringari, Theory of ultracold atomic Fermi gases, *Rev. Mod. Phys.* **80**, 1215 (2008).
- [7] A. Cichy and R. Micnas, The spin-imbalanced attractive Hubbard model in  $d = 3$ : Phase diagrams and BCS-BEC crossover at low filling, *Ann. Phys.* **347**, 207 (2014).
- [8] X.-W. Guan, M. T. Batchelor, and C. Lee, Fermi gases in one dimension: From Bethe ansatz to experiments, *Rev. Mod. Phys.* **85**, 1633 (2013).
- [9] P. Dyke, E. D. Kuhnle, S. Whitlock, H. Hu, M. Mark, S. Hoinka, M. Lingham, P. Hannaford, and C. J. Vale, Crossover from 2D to 3D in a Weakly Interacting Fermi Gas, *Phys. Rev. Lett.* **106**, 105304 (2011).

- [10] A. T. Sommer, L. W. Cheuk, M. J. H. Ku, W. S. Bakr, and M. W. Zwierlein, Evolution of Fermion Pairing from Three to Two Dimensions, *Phys. Rev. Lett.* **108**, 045302 (2012).
- [11] M. G. Ries, A. N. Wenz, G. Zürn, L. Bayha, I. Boettcher, D. Kedar, P. A. Murthy, M. Neidig, T. Lompe, and S. Jochim, Observation of Pair Condensation in the Quasi-2D BEC-BCS Crossover, *Phys. Rev. Lett.* **114**, 230401 (2015).
- [12] P. A. Murthy, I. Boettcher, L. Bayha, M. Holzmann, D. Kedar, M. Neidig, M. G. Ries, A. N. Wenz, G. Zürn, and S. Jochim, Observation of the Berezinskii-Kosterlitz-Thouless Phase Transition in an Ultracold Fermi Gas, *Phys. Rev. Lett.* **115**, 010401 (2015).
- [13] M. Feld, B. Froehlich, E. Vogt, M. Koschorreck, and M. Köhl, Observation of a pairing pseudogap in a two-dimensional Fermi gas, *Nature* **480**, 75 (2011).
- [14] R. Micnas, J. Ranninger, and S. Robaszkiewicz, Superconductivity in narrow-band systems with local nonretarded attractive interactions, *Rev. Mod. Phys.* **62**, 113 (1990).
- [15] Q. J. Chen, I. Kosztin, B. Jankó, and K. Levin, Superconducting transitions from the pseudogap state:  $d$ -wave symmetry, lattice, and low-dimensional effects, *Phys. Rev. B* **59**, 7083 (1999).
- [16] W. Hofstetter, J. I. Cirac, P. Zoller, E. Demler, and M. D. Lukin, High-Temperature Superfluidity of Fermionic Atoms in Optical Lattices, *Phys. Rev. Lett.* **89**, 220407 (2002); W. V. Liu, F. Wilczek, and P. Zoller, Spin-dependent Hubbard model and a quantum phase transition in cold atoms, *Phys. Rev. A* **70**, 033603 (2004); M. A. Cazalilla, A. F. Ho, and T. Giamarchi, Two-component Fermi Gas on Internal-State-Dependent Optical Lattices, *Phys. Rev. Lett.* **95**, 226402 (2005); T. Koponen, J. Kinnunen, J.-P. Martikainen, L. M. Jensen, and P. Törmä, Fermion pairing with spin-density imbalance in an optical lattice, *New J. Phys.* **8**, 179 (2006); A. Moreo and D. J. Scalapino, Cold Attractive Spin Polarized Fermi Lattice Gases and the Doped Positive  $U$  Hubbard Model, *Phys. Rev. Lett.* **98**, 216402 (2007).
- [17] C.-C. Chien, Y. He, Q. Chen, and K. Levin, Superfluid-insulator transitions at noninteger filling in optical lattices of fermionic atoms, *Phys. Rev. A* **77**, 011601(R) (2008); C.-C. Chien, Q. J. Chen, and K. Levin, Fermions with attractive interactions on optical lattices and implications for correlated systems, *ibid.* **78**, 043612 (2008).
- [18] M. Iskin and C. J. Williams, Population-imbalanced fermions in harmonically trapped optical lattices, *Phys. Rev. A* **78**, 011603(R) (2008); Z. Cai, Y. Wang, and C. Wu, Stable Fulde-Ferrell-Larkin-Ovchinnikov pairing states in 2D and 3D optical lattices, *ibid.* **83**, 063621 (2011); T. Gottwald and P. G. J. van Dongen, Ground-state properties of an asymmetric Hubbard model for unbalanced ultracold fermionic quantum gases, *Eur. Phys. J. B* **61**, 277 (2008); Y. Chen, Z. D. Wang, F. C. Zhang, and C. S. Ting, Exploring exotic superfluidity of polarized ultracold fermions in optical lattices, *Phys. Rev. B* **79**, 054512 (2009); B. Wang, H.-D. Chen, and S. Das Sarma, Quantum phase diagram of fermion mixtures with population imbalance in one-dimensional optical lattices, *Phys. Rev. A* **79**, 051604(R) (2009); Y. L. Loh and N. Trivedi, Detecting the Elusive Larkin-Ovchinnikov Modulated Superfluid Phases for Imbalanced Fermi Gases in Optical Lattices, *Phys. Rev. Lett.* **104**, 165302 (2010); X. Cui and Y. Wang, Polarized Fermi gases in asymmetric optical lattices, *Phys. Rev. A* **81**, 023618 (2010).
- [19] A.-Hai Chen and G. Xianlong, Pure Fulde-Ferrell-Larkin-Ovchinnikov state in optical lattices, *Phys. Rev. B* **85**, 134203 (2012); R. Mendoza, M. Fortes, M. A. Solís, and Z. Koinov, Superfluidity of a spin-imbalanced Fermi gas in a three-dimensional optical lattice, *Phys. Rev. A* **88**, 033606 (2013).
- [20] M. O. J. Heikkinen, D.-H. Kim, M. Troyer, and P. Törmä, Nonlocal Quantum Fluctuations and Fermionic Superfluidity in the Imbalanced Attractive Hubbard Model, *Phys. Rev. Lett.* **113**, 185301 (2014); R. Peters and J. Bauer, Local origin of the pseudogap in the attractive Hubbard model, *Phys. Rev. B* **92**, 014511 (2015); S. Kitamura and H. Aoki,  $\eta$ -pairing superfluid in periodically driven fermionic Hubbard model with strong attraction, *ibid.* **94**, 174503 (2016).
- [21] S.-J. Gu, R. Fan, and H.-Q. Lin, Ground state of a mixture of two species of fermionic atoms in a one-dimensional optical lattice, *Phys. Rev. B* **76**, 125107 (2007); A. E. Feiguin and F. Heidrich-Meisner, Pairing states of a polarized Fermi gas trapped in a one-dimensional optical lattice, *ibid.* **76**, 220508(R) (2007); M. Rizzi, M. Polini, M. A. Cazalilla, M. R. Bakhtiari, M. P. Tosi, and R. Fazio, Fulde-Ferrell-Larkin-Ovchinnikov pairing in one-dimensional optical lattices, *ibid.* **77**, 245105 (2008); M. R. Bakhtiari, M. J. Leskinen, and P. Törmä, Spectral Signatures of the Fulde-Ferrell-Larkin-Ovchinnikov Order Parameter in One-Dimensional Optical Lattices, *Phys. Rev. Lett.* **101**, 120404 (2008); T. Roscilde, C. D. E. Boschi, and M. Dalmonte, Pairing, crystallization and string correlations of mass-imbalanced atomic mixtures in one-dimensional optical lattices, *Europhys. Lett.* **97**, 23002 (2012); V. V. Franca, D. Hördlein, and A. Buchleitner, Fulde-Ferrell-Larkin-Ovchinnikov critical polarization in one-dimensional fermionic optical lattices, *Phys. Rev. A* **86**, 033622 (2012).
- [22] P. Fulde and R. A. Ferrell, Superconductivity in a strong spin-exchange field, *Phys. Rev.* **135**, A550 (1964).
- [23] A. I. Larkin and Y. N. Ovchinnikov, Inhomogeneous state of superconductors, *Sov. Phys. JETP* **20**, 762 (1965) [*Zh. Eksp. Teor. Fiz.* **47**, 1136 (1964)].
- [24] J. P. A. Devreese, S. N. Klimin, and J. Tempere, Resonant enhancement of the Fulde-Ferrell-Larkin-Ovchinnikov state in three dimensions by a one-dimensional optical potential, *Phys. Rev. A* **83**, 013606 (2011); J. P. A. Devreese, M. Wouters, and J. Tempere, Controlling the pair momentum of the Fulde-Ferrell-Larkin-Ovchinnikov state in a three-dimensional Fermi gas through a one-dimensional periodic potential, *ibid.* **84**, 043623 (2011); J. P. A. Devreese, S. Klimin, M. Wouters, and J. Tempere, The Fulde-Ferrell-Larkin-Ovchinnikov state in a 3D Fermi gas subjected to a 1D periodic potential, *Mod. Phys. Lett. B* **26**, 1230014 (2012).
- [25] Q. J. Chen, I. Kosztin, B. Jankó, and K. Levin, Pairing Fluctuation Theory of Superconducting Properties in Underdoped to Overdoped Cuprates, *Phys. Rev. Lett.* **81**, 4708 (1998).
- [26] Q. J. Chen, Y. He, C.-C. Chien, and K. Levin, Theory of superfluids with population imbalance: Finite-temperature and BCS-BEC crossover effects, *Phys. Rev. B* **75**, 014521 (2007).
- [27] Q. J. Chen, Y. He, C.-C. Chien, and K. Levin, Theory of radio frequency spectroscopy experiments in ultracold Fermi gases and their relation to photoemission experiments in the cuprates, *Rep. Prog. Phys.* **72**, 122501 (2009).

- [28] Q. J. Chen, Zero-density-limit extrapolation of the superfluid transition temperature in a unitary atomic Fermi gas on a lattice, *Phys. Rev. A* **86**, 023610 (2012).
- [29] L. F. Zhang, Y. M. Che, J. B. Wang, and Q. J. Chen, Exotic superfluidity and pairing phenomena in atomic Fermi gases in mixed dimensions, *Sci. Rep.* **7**, 12948 (2017).
- [30] Q. J. Chen and J. B. Wang, Pseudogap phenomena in ultracold atomic Fermi gases, *Front. Phys.* **9**, 539 (2014).
- [31] E. J. Mueller, Review of pseudogaps in strongly interacting Fermi gases, *Rep. Prog. Phys.* **80**, 104401 (2017).
- [32] A. L. Fetter and J. D. Walecka, *Quantum Theory of Many-Particle Systems* (McGraw-Hill, San Francisco, 1971).
- [33] D. J. Thouless, Perturbation theory in statistical mechanics and the theory of superconductivity, *Ann. Phys.* **10**, 553 (1960).
- [34] T. Timusk and B. Statt, The pseudogap in high-temperature superconductors: An experimental survey, *Rep. Prog. Phys.* **62**, 61 (1999).
- [35] P. Nozières and S. Schmitt-Rink, Bose condensation in an attractive fermion gas: From weak to strong coupling superconductivity, *J. Low Temp. Phys.* **59**, 195 (1985).
- [36] V. Makhalov, K. Martiyanov, and A. Turlapov, Ground-State Pressure of Quasi-2D Fermi and Bose Gases, *Phys. Rev. Lett.* **112**, 045301 (2014); K. Fenech, P. Dyke, T. Pepler, M. G. Lingham, S. Hoinka, H. Hu, and C. J. Vale, Thermodynamics of an Attractive 2D Fermi Gas, *ibid.* **116**, 045302 (2016); I. Boettcher, L. Bayha, D. Kedar, P. A. Murthy, M. Neidig, M. G. Ries, A. N. Wenz, G. Zürn, S. Jochim, and T. Ess, Equation of State of Ultracold Fermions in the 2D BEC-BCS Crossover Region, *ibid.* **116**, 045303 (2016); K. Hueck, N. Luick, L. Sobirey, J. Siegl, T. Lompe, and H. Moritz, Two-Dimensional Homogeneous Fermi Gases, *ibid.* **120**, 060402 (2018).
- [37] G. Bertainia and S. Giorgini, BCS-BEC Crossover in a Two-Dimensional Fermi Gas, *Phys. Rev. Lett.* **106**, 110403 (2011); H. Shi, S. Chiesa, and S. Zhang, Ground-state properties of strongly interacting Fermi gases in two dimensions, *Phys. Rev. A* **92**, 033603 (2015); L. He, H. Lü, G. Cao, H. Hu, and X.-J. Liu, Quantum fluctuations in the BCS-BEC crossover of two-dimensional Fermi gases, *ibid.* **92**, 023620 (2015); U. Toniolo, B. C. Mulkerin, C. J. Vale, X.-J. Liu, and H. Hu, Dimensional crossover in a strongly interacting ultracold atomic Fermi gas, *ibid.* **96**, 041604(R) (2017); H. Hu, B. C. Mulkerin, U. Toniolo, L. He, and X.-J. Liu, Reduced Quantum Anomaly in a Quasi-Two-Dimensional Fermi Superfluid: Significance of the Confinement-Induced Effective Range of Interactions, *Phys. Rev. Lett.* **122**, 070401 (2019).
- [38] V. L. Berezinskii, Destruction of long-range order in one-dimensional and two-dimensional systems possessing a continuous symmetry group II. Quantum systems, *Sov. Phys. JETP* **34**, 610 (1972); J. M. Kosterlitz and D. J. Thouless, Ordering, metastability and phase transitions in two-dimensional systems, *J. Phys. C: Solid State* **6**, 1181 (1973).
- [39] M. Iskin and C. A. R. Sá de Melo, Evolution from BCS to Berezinskii-Kosterlitz-Thouless Superfluidity in One-Dimensional Optical Lattices, *Phys. Rev. Lett.* **103**, 165301 (2009).
- [40] J. R. Schrieffer, *Theory of Superconductivity*, 3rd ed. (Perseus Books, Reading, MA, 1983).
- [41] J. F. Annett, N. Goldenfeld, and A. J. Leggett, Experimental constraints on the pairing state of the cuprate superconductors: An emerging consensus, in *Physical Properties of High Temperature Superconductors V*, edited by D. M. Ginsberg (World Scientific, Singapore, 1996), pp. 375–461.
- [42] Q. J. Chen and J. R. Schrieffer, Pairing fluctuation theory of high- $T_c$  superconductivity in the presence of nonmagnetic impurities, *Phys. Rev. B* **66**, 014512 (2002); Q. J. Chen and K. Levin, Phenomenological theory of the protected nodes and collapse of the Fermi arcs in underdoped cuprate superconductors, *ibid.* **78**, 020513(R) (2008).
- [43] I. Kosztin, Q. J. Chen, B. Jankó, and K. Levin, Relationship between the pseudo- and superconducting gaps: Effects of residual pairing correlations below  $T_c$ , *Phys. Rev. B* **58**, R5936 (1998).
- [44] Q. J. Chen, Generalization of BCS theory to short coherence length superconductors: A BCS–Bose–Einstein crossover scenario, Ph.D. thesis, University of Chicago, 2000, [arXiv:1801.06266](https://arxiv.org/abs/1801.06266).
- [45] The minimum of  $T_c$  occurs for simple reasons. In homogeneous 3D continuum,  $T_c$  at unitarity in both the present and the Nozière–Schmitt-Rink [35] schemes are known to be larger than its BEC asymptote,  $0.218T_F$ . At the same time, the effective pair mass approaches  $M_{\parallel} = 2m$  from above as the pairing strength grows, which requires that  $T_c$  approach its BEC asymptote from below. Therefore, a minimum in  $T_c$  naturally occurs in between. We find that it corresponds to where the Fermi surface shrinks to zero. Indeed, on the fermionic side, as the pairing strength increases, the shrinking Fermi surface leads to a decreasing density of states at the Fermi level and thus causes  $T_c$  to decrease, until the Fermi surface no longer exists. Beyond this point, all fermions form pairs, and then the  $T_c$  behavior is dominated by the effective pair mass, which decreases toward  $2m$  so that  $T_c$  rises again gradually (see Ref. [15] for details). While this minimum is associated with the boundary separating the fermionic and bosonic regimes, it does not, however, indicate a phase transition for the  $s$ -wave pairing. For nodal superfluids such as  $p$ - and  $d$ -wave superconductors,  $\mu = 0$  leads to disappearance of the nodes and thus to discontinuities in compressibility, which has been referred to as a quantum phase transition [55].
- [46] L. F. Zhang, J. B. Wang, Y. Yu, and Q. J. Chen, Ultra high temperature superfluidity in ultracold atomic Fermi gases with mixed dimensionality, *Sci. China Phys. Mech. Astron.* **63**, 227421 (2020).
- [47] A. Larkin and A. Varlamov, *Theory of Fluctuations in Superconductors*, International Series of Monographs on Physics (Oxford University Press, Oxford, 2009).
- [48] R. Boyack, Q. J. Chen, A. A. Varlamov, and K. Levin, Cuprate diamagnetism in the presence of a pseudogap: Beyond the standard fluctuation formalism, *Phys. Rev. B* **97**, 064503 (2018).
- [49] P. Bloom, Two-dimensional fermi gas, *Phys. Rev. B* **12**, 125 (1975).
- [50] M. Randeria, J.-M. Duan, and L.-Y. Shieh, Superconductivity in a two-dimensional Fermi gas: Evolution from Cooper pairing to Bose condensation, *Phys. Rev. B* **41**, 327 (1990).
- [51] D. S. Petrov and G. V. Shlyapnikov, Interatomic collisions in a tightly confined Bose gas, *Phys. Rev. A* **64**, 012706 (2001).

- [52] Q. J. Chen and K. Levin, Population of Closed-Channel Molecules in Trapped Fermi Gases with Broad Feshbach Resonances, *Phys. Rev. Lett.* **95**, 260406 (2005).
- [53] Q. J. Chen, J. B. Wang, L. Sun, and Y. Yu, Unusual destruction and enhancement of superfluidity of atomic Fermi gases by population imbalance in a one-dimensional optical lattice, *Chin. Phys. Lett.* **37**, 053702 (2020).
- [54] C.-C. Chien, Q. J. Chen, Y. He, and K. Levin, Intermediate Temperature Superfluidity in a Fermi Gas with Population Imbalance, *Phys. Rev. Lett.* **97**, 090402 (2006).
- [55] S. S. Botelho and C. A. R. Sá de Melo, Quantum phase transition in the BCS-to-BEC evolution of  $p$ -wave Fermi gases, *J. Low Temp. Phys.* **140**, 409 (2005).